The Astrophysical Journal Letters, 843:L1 (6pp), 2017 July 1 https://doi.org/10.3847/2041-8213/aa79a7

The Braking Index of Millisecond Magnetars

Paul D. Lasky[1,2], Cristiano Leris[1], Antonia Rowlinson[3,4], and Kostas Glampedakis[5,6]
[1] Monash Centre for Astrophysics, School of Physics and Astronomy, Monash University, Vic 3800, Australia; paul.lasky@monash.edu
[2] OzGrav: The ARC Centre of Excellence for Gravitational-wave Discovery, Hawthorn, Vic 3122, Australia
[3] Anton Pannekoek Institute, University of Amsterdam, Postbus 94249, NL-1090 GE, Amsterdam, The Netherlands
[4] Netherlands Institute for Radio Astronomy (ASTRON), P.O. Box 2, NL-7990 AA Dwingeloo, The Netherlands
[5] Departamento de Física, Universidad de Murcia, E-30100 Murcia, Spain
[6] Theoretical Astrophysics, University of Tübingen, Auf der Morgenstelle 10, D-72076 Tübingen, Germany
Received 2017 May 28; revised 2017 June 13; accepted 2017 June 14; published 2017 June 23

Abstract

We make the first measurement of the braking index n of two putative millisecond magnetars born in short gamma-ray bursts. We measure $n = 2.9 \pm 0.1$ and $n = 2.6 \pm 0.1$ for millisecond magnetars born in GRB 130603B and GRB 140903A, respectively. The neutron star born in GRB 130603B has the only known a braking index consistent with the fiducial $n = 3$ value. This value is ruled out with 99.95% confidence for GRB 140903A. We discuss possible causes of $n < 3$ braking indices in millisecond magnetars, showing that several models can account for the measurement of the braking index in GRB 140903A, while it is more difficult to account for a braking index consistent with $n = 3$.

Key words: gamma-ray burst: individual (GRB 130603B, GRB 140903A) – stars: magnetars – stars: neutron

1. Introduction

Observations of gamma-ray bursts and superluminous supernovae show evidence for ongoing energy injection following the prompt emission (Nousek et al. 2006; O'Brien et al. 2006; Zhang et al. 2006), which is commonly attributed to the birth of rapidly rotating, highly magnetized neutron stars, known as a millisecond magnetars (e.g., Rowlinson et al. 2013; Lü & Zhang 2014; Inserra et al. 2016). The spin-down of the nascent neutron star drives high-energy emissions that are observed as long-lasting ($\gtrsim 10^3$ s) X-ray plateaus.

The fiducial millisecond magnetar model relates the evolution of the star's spin frequency $\Omega(t)$ to the X-ray light curve (Zhang & Mészáros 2001; Metzger et al. 2011). The original model assumes that the rapidly rotating star loses angular momentum through a combination of gravitational waves and electromagnetic radiation, although the amount of energy lost to gravitational-wave emission is small compared to electromagnetic losses (Ho 2016; Lasky & Glampedakis 2016; Moriya & Tauris 2016). In general, the spin-down of a neutron star can be described by the torque equation

$$\dot{\Omega} = -k\Omega^n, \tag{1}$$

where k is a constant of proportionality and n is the braking index.

An unchanging, dipolar magnetic field in vacuo implies a theoretical braking index of $n = 3$ (Ostriker & Gunn 1969). This fiducial assumption is built into the millisecond magnetar model and leads to a prediction that the light curve luminosity decays as $L \propto t^{-2}$ at late times (Zhang & Mészáros 2001). Gamma-ray burst and superluminous supernova light curves are usually fit assuming a braking index of $n = 3$ (e.g., Troja et al. 2007; Chatzopoulos et al. 2013; Rowlinson et al. 2013).

In principle, Equation (1) should equally apply to the spin-down of rotation-powered pulsars. Empirically, though, not a single pulsar with a measured braking index is consistent with $n = 3$, with all but one falling below $n \lesssim 3$ (see Archibald et al. 2016; Clark et al. 2016; Marshall et al. 2016 and references therein). More realistic calculations of pulsars and their magnetospheres ubiquitously predict $n \lesssim 3$ (e.g., Melatos 1997).

In this Letter, we make the first measurement of the braking index of two millisecond magnetars. In particular, short gamma-ray bursts GRB 130603B and GRB 140903A, which were both observed with the *Swift* telescope and subsequently with *XMM* and *Chandra*, respectively. These late-time observations ($\gtrsim 10^5$ s after the initial burst) allow us to make accurate measurements of the power-law decay of the light curve, and hence get tight constraints on the braking indices for the millisecond magnetars.[7]

We find that the braking index for the millisecond magnetar born in GRB 130603B is $n = 2.9 \pm 0.1$ (1σ confidence level), and hence is consistent with $n = 3$. On the other hand, the millisecond magnetar born in GRB 140903A has $n = 2.6 \pm 0.1$, ruling out $n = 3$ with 99.95% confidence. We discuss physical mechanisms that can cause sub-three braking indices, finding that these naturally arise from physically realistic models of post-merger remnants.

2. Observations and Model

2.1. Generalized Millisecond Magnetar Model

As a neutron star spins down, rotational kinetic energy is lost from the system, $E = \frac{1}{2}I\Omega^2$, where I is the star's moment of inertia. The time derivative of this equation gives the rate of change of energy loss, a certain fraction of which is converted into X-rays. The X-ray luminosity is therefore $L = -\eta\dot{E} = -\eta\Omega\dot{\Omega}$, where η is the efficiency in converting spin-down energy into X-rays. We assume throughout that η is not a function of time, a point we discuss further below. Integrating Equation (1) gives the evolution of $\Omega(t)$, implying

[7] The only other short GRB with such late-time observations, albeit with only *Swift*, is GRB 051221A; however, Lü et al. (2015) claim that the temporal and spectral properties pre- and post-break are consistent with an external forward shock, with only the plateau phase being due to continuous energy injection.

the luminosity is

$$L(t) = L_0\left(1 + \frac{t}{\tau}\right)^{\frac{1+n}{1-n}}. \quad (2)$$

Here, $L_0 \equiv \eta I k \Omega_0^{1+n}$ is the initial luminosity, $\Omega_0 \equiv \Omega(t=0)$, and $\tau \equiv \Omega_0^{1-n}/[(n-1)k]$ is the spin-down timescale of the system.

Equation (2) shows the characteristic plateau $L = L_0$ behavior for early times $t \ll \tau$ and a power-law decay $L \propto t^{(1+n)/(1-n)}$ for $t \gg \tau$. When $n = 3$, Equation (2) recovers the familiar late-time $L \propto t^{-2}$ behavior where τ is the electromagnetic spin-down timescale (Zhang & Mészáros 2001). In this limit, the spin-down timescale becomes the familiar electromagnetic spin-down timescale $\tau = \tau_{\rm em} \equiv 3c^3 I/(B_p^2 R^6 \Omega_0^2)$, where B_p is the dipole, poloidal component of the star's magnetic field, and R is the stellar radius. Normalizing to typical millisecond magnetar parameters (Lasky et al. 2014),

$$\tau_{\rm em} \approx 5 \times 10^3 \left(\frac{B_p}{10^{15}\,{\rm G}}\right)^{-2}\left(\frac{P}{1\,{\rm ms}}\right)^2 {\rm s}, \quad (3)$$

where P is the spin period.

It is worth noting that Equation (2) is different from the "standard" derivation in the literature for when the spin-down is dominated by gravitational-wave emission. In that case, the braking index is $n = 5$, implying from Equation (2) that the luminosity decays as $t^{-3/2}$, instead of the oft-quoted t^{-1} (e.g., Zhang & Mészáros 2001; Lasky & Glampedakis 2016). The derivation of t^{-1} assumes that only the electromagnetic dipolar component of the spin-down energy contributes to the X-ray light curve, whereas here the only assumption that has been made is that some fixed fraction η of the spin-down energy is converted into X-rays.

In this Letter, we fit Equation (2), combined with an initial power-law decay $L = At^{-\alpha}$ describing the transition between the prompt emission and the plateau phase (Rowlinson et al. 2013) to the data (described below). We use Bayesian nested sampling, which provides us with joint posterior probability densities for $\{L_0, \tau, n, A, \alpha\}$.

2.2. GRB 130603B

The short-duration GRB 130603B generated much interest as it was the first credible detection of a kilonova associated with a short GRB (Berger et al. 2013; Tanvir et al. 2013). The initial burst (Melandri et al. 2013) was picked up by the Burst Alert Telescope (BAT; Barthelmy et al. 2005) on board *Swift* with a duration of $T_{90} = 0.18 \pm 0.02$ s in the 15–350 keV band (Barthelmy et al. 2013). The X-ray Telescope (XRT; Burrows et al. 2005) on board *Swift* detected a corresponding fading X-ray source 59 s after the initial burst (Kennea et al. 2013). A late-time excess was also observed with *XMM-Newton* ≈2.7 and ≈6.5 days after the initial burst (Fong et al. 2014).

The millisecond magnetar model has been invoked to explain both XRT and *XMM* X-ray excesses (Fan et al. 2013; de Ugarte Postigo et al. 2014; Fong et al. 2014). These papers all used the fiducial magnetar model with a braking index of $n = 3$, allowing the magnetic field and initial spin period to be measured.

Here, we fit the more general magnetar model to the same data as that of Fong et al. (2014) and de Ugarte Postigo et al. (2014), allowing for a variable breaking index. The top panel of

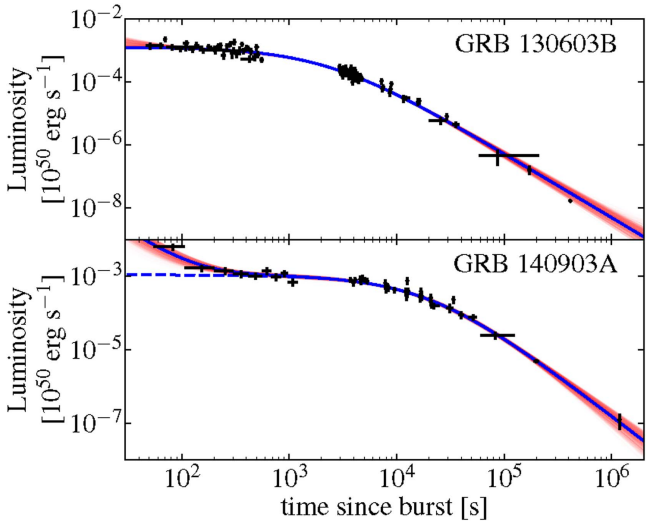

Figure 1. X-ray light curves for GRB 130603B (top panel) and GRB 140903A (bottom panel). In each panel, the black points represent the data (see Sections 2.2 and 2.3 for details). The solid blue curve is the best-fit millisecond magnetar model, where the braking index (n; see Equation (2)) is included in the fit. The dashed blue curve is the best-fit millisecond magnetar model not including the contribution from the initial power-law decay. The dark red band is the superposition of many light curve models, where each curve is drawn from a single posterior sample.

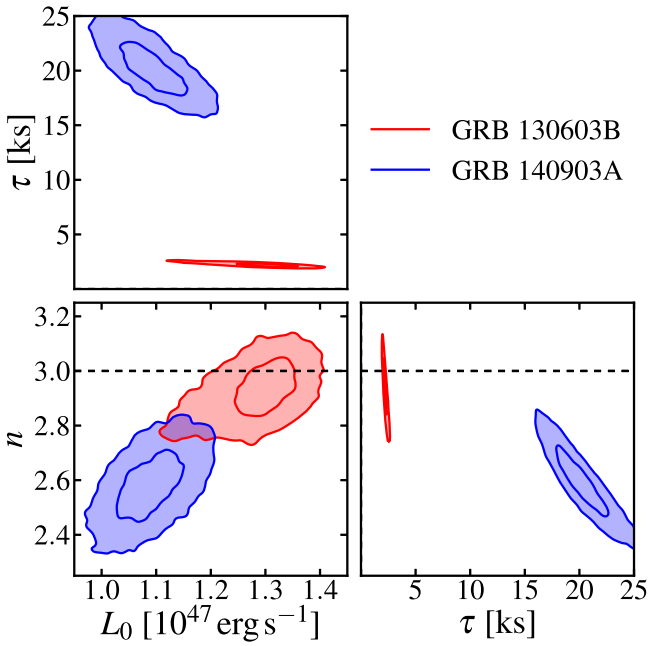

Figure 2. Posterior probability distributions for the parameters in Equation (2) for GRB 130603B (red) and GRB 140903A (blue). The contours show the 1σ and 2σ confidence intervals, and the dashed line indicates the fiducial value of $n = 3$.

Figure 1 shows the XRT and *XMM* data, together with our fit using Equation (2) and an initial power law that fits the prompt emission. The solid blue curve shows the maximum-likelihood model, while the dark red band is the superposition of many light curve models, where each model is drawn from a single posterior sample.

In Figure 2 we show a corner plot of the posterior probability distributions for the parameters in the magnetar model; the red contours show the posterior distributions for GRB 130603B. In Figure 3, we plot the one-dimensional marginalized posterior

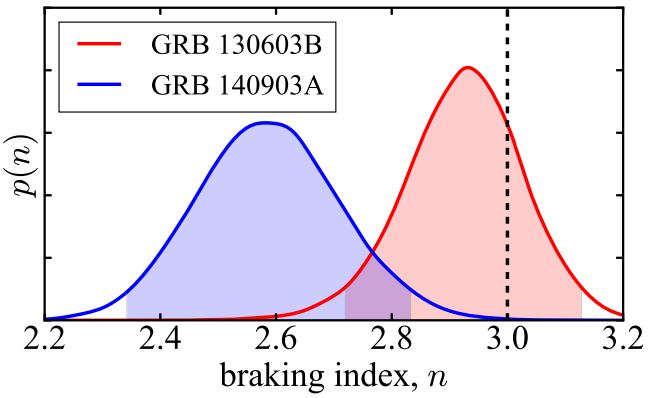

Figure 3. One-dimensional marginalized posterior distributions for the braking index n for GRB 130603B (red) and GRB 140903A (blue). The shaded regions show the 2σ confidence intervals, and the dashed black line indicates the fiducial value of $n = 3$.

distribution for the braking index, n. The red curve representing the braking index for GRB 130603B shows consistency with the fiducial $n = 3$ braking index, with $n = 2.9 \pm 0.1$, where the uncertainties correspond to 1σ confidence intervals.

2.3. GRB 140903A

GRB 140903A triggered BAT on 2014 September 3 (Cummings et al. 2014; Palmer et al. 2014), with XRT observations of the GRB field 74 s after the BAT trigger (de Pasquale et al. 2014). Two observations with the *Chandra X-ray Observatory* were taken ≈3 and ≈15 days following the initial BAT trigger, respectively (Troja et al. 2016). The X-ray and other multi-wavelength observations of the GRB afterglow have been used to determine an achromatic jet-break, and hence infer the existence of a jet with a narrow opening angle of $\theta \approx 5^\circ$ (Troja et al. 2016; Zhang et al. 2017). Moreover, the *Swift* and *Chandra* X-ray plateau and power-law decay have been well modeled within the fiducial $n = 3$ magnetar model (Zhang et al. 2017).

We again fit the more general magnetar model to the same X-ray data used in Troja et al. (2016) and Zhang et al. (2017). The bottom panel of Figure 1 shows the XRT and late-time *Chandra* observations, together with our fit. The solid blue curve again shows the maximum-likelihood model, and the dark red band shows the superposition of many light curves, each drawn from single posterior samples.

The posterior probability distributions for the parameters of the millisecond magnetar model are shown as the blue contours in Figure 2. The one-dimensional marginalized posterior distribution for the braking index is shown in blue in Figure 3, which gives $n = 2.6 \pm 0.1$. The fiducial value of $n = 3$ is ruled out with 99.95% confidence.

2.4. Comparison with Pulsars

In Figure 4, we plot the braking indices for all known pulsars where the long-term spin-down is believed to be electromagnetically dominated (see Archibald et al. 2016; Clark et al. 2016 and references therein). For comparison, we also plot the braking indices of the two neutron stars purportedly born in GRB 130603B and GRB 140903A. The range of braking indices for pulsars spreads between $1 \lesssim n \lesssim 3.15$. Clearly, there are not enough data to determine whether the sample of

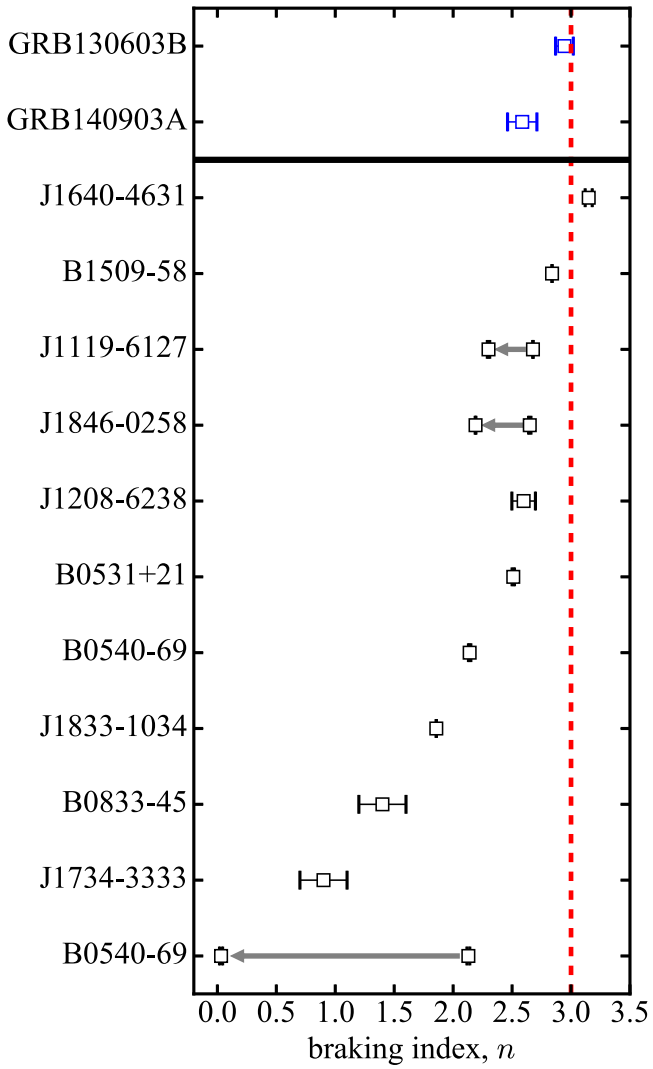

Figure 4. Measured millisecond magnetar and pulsar braking indices. The pulsar braking indices data are taken from Archibald et al. (2016), Clark et al. (2016), Marshall et al. (2016), and references therein. Gray arrows represent changing braking indices seen in single pulsars between different spin-down states.

GRB braking indices are statistically consistent with the distribution of pulsar braking indices with high confidence; we leave this as a topic for future work.

Intriguingly, Figure 4 shows that the neutron star born in GRB 130603B has the only known braking index consistent with the fiducial $n = 3$ value. As we discuss below, it is relatively simple to devise models that explain $n \lesssim 3$; the question therefore becomes: what is unique about the neutron star in GRB 130603B that makes it consistent with $n = 3$?

3. Theoretical Explanation

The fiducial $n = 3$ braking index is the one associated with the classic oblique rotator model in vacuo (Ostriker & Gunn 1969). The markedly more realistic model of Goldreich & Julian (1969), based on a charged-filled and force-free magnetosphere, also leads to the same prediction (see Spitkovsky 2008, for a review). The departure of observed pulsar braking indices from the fiducial value can therefore be

taken as evidence of additional physical processes affecting the spin-down of these objects.

The literature posits an assortment of models that could explain the observed anomalous $n \lesssim 3$ braking indices, but it is an open question as to which of those are relevant for the timescales, magnetic field strengths, and environmental conditions that are being discussed here. Here, we focus on the various possibilities that could be of relevance for a millisecond magnetar system such as GRB 140903A. And as we discuss, these may *not* be the same mechanisms usually invoked for explaining anomalous braking indices of known pulsars.

3.1. Modified Magnetosphere Spin-down

A millisecond magnetar formed in the aftermath of a binary neutron star merger is likely endowed with a very strong toroidal magnetic field $\gtrsim 10^{15}$ G. This arises as both differential rotation of the body and the magneto-rotational instability work in concert to amplify the field and wind up its lines; these processes are expected to be present in the first $\sim$10–100 ms following the merger (e.g., Rezzolla et al. 2011; Kiuchi et al. 2014). The induced magnetic field eventually quenches differential rotation on an Alfvén timescale $\ll 1$ s (Baumgarte et al. 2000; Shapiro 2000). Therefore, after the initially chaotic period, the star settles to a rapidly, but rigidly, rotating fluid ball with a strong, internal magnetic field.

The generated field is dynamically unstable and rapidly rearranges itself to a state of hydromagnetic equilibrium where both poloidal and toroidal components are of comparable strength (e.g., Braithwaite 2009). The global magnetic field rearrangement is likely to involve the bubbling up of toroidal magnetic flux to the stellar surface and into the magnetosphere (e.g., Kiuchi et al. 2011). The system therefore acquires a *twisted* magnetosphere consisting of a strong mixed poloidal–toroidal field. This type of magnetosphere, originally modeled by Thompson et al. (2002), is also believed to form in garden-variety magnetars (see Turolla et al. 2015 and references therein). Such twisted magnetospheres increase the spin-down torque in comparison to orthogonal vacuum dipoles, implying reduced values of the braking index, i.e., $n \lesssim 3$ (Thompson et al. 2002). The amount of reduction is not unique, but largely depends on the field's radial profile and the degree of twist, with higher twist leading to a smaller braking index.

An entirely different magnetospheric modification for producing an $n < 3$ spin-down has been proposed by Contopoulos & Spitkovsky (2006). In this model, which assumes a dipole force/twist-free magnetosphere, a distinction is made between the light-cylinder radius $R_{\rm lc} = c/\Omega$ (the cylindrical radius at which a magnetosphere rigidly corotating with the star would exceed the speed of light) and the separatrix radius $R_{\rm c}$ between open and closed field lines.

Although the standard assumption is that of $R_{\rm lc} = R_{\rm c}$, this may not be a strictly imposed physical necessity; $R_{\rm c}$ could lag behind $R_{\rm lc}$ if the spin-down is fast and the magnetic field line reconnection cannot keep up with the outward migrating light-cylinder (for details, see Contopoulos & Spitkovsky 2006). Such a scenario could be strongly favored in a millisecond magnetar, implying the spin-down torque is enhanced as a result of the open field lines' larger aperture. A braking index of $n < 3$ therefore naturally emerges.

3.2. Magnetic Axis Evolution and Other Mechanisms

Another possible explanation for $n \lesssim 3$ braking indices relates to the evolution of the angle α between the star's rotation axis and its surface dipole magnetic field axis.

This mechanism, for example, has been invoked to explain the braking index of the Crab pulsar (Lyne et al. 2015). Here, the k term in Equation (1) is a function of time, and the braking index can be approximated as $n = 3 + 2\Omega\dot{\alpha}/(\dot{\Omega}\tan\alpha)$. Clearly, $\dot{\alpha} > 0$ leads to a braking index $n < 3$.

The time evolution of α largely depends on whether the dipole field can be considered rigidly attached to the star's "body frame"—i.e., the deformed shape induced by the strong toroidal component. According to standard oblique rotator theory (Goldreich 1970), the electromagnetic torque due to the exterior field drives the symmetry axis of the deformation toward (away from) the spin axis on a spin-down timescale $\tau_{\rm em}$ if its direction with respect to the dipole axis makes an angle smaller (larger) than $\approx 55°$. Assuming a fixed relative orientation between the surface dipole and internal toroidal field symmetry axes, the desired $\dot{\alpha} > 0$ situation arises provided the dipole axis is significantly misaligned ($\gtrsim 55°$) with respect to the spin axis since the latter axis is expected to lie close to the toroidal field's symmetry axis.

The evolution of the relative orientation between the spin and deformation axes also couples to the emitted gravitational waves (Cutler & Jones 2001). Unlike the previous case, however, gravitational radiation always drives the two axes toward alignment, on a timescale of $\tau_{\rm gw} \approx 2 \times 10^4 (\epsilon_B/10^{-3})^{-2} (P/1\ {\rm ms})^4$ s, where $\epsilon_{\rm B}$ is the magnetic-field-induced stellar ellipticity. This is long compared to the electromagnetic spin-down timescale—cf. Equation (3)—unless the ellipticity is $\epsilon \gtrsim 10^{-2}$, which is all but ruled out for systems in which the ellipticity can be measured (Lasky & Glampedakis 2016).

A natural way to drive an $\dot{\alpha} > 0$ evolution is through the so-called "spin-flip" instability (e.g., Cutler 2002). Here, the strong internal toroidal field causes the star to become a prolate spheroid in the first few seconds after birth. Such an arrangement is unstable, and under the action of internal dissipation (in the present case bulk viscosity), the system is driven toward a state where the spin and toroidal symmetry axes are mutually orthogonal. If the dipole field is assumed to be "locked" to the toroidal component, then this orthogonalization implies $\dot{\alpha} > 0$.

The spin-flip could be a viable mechanism for modifying the braking index provided its timescale is comparable to the spin-down timescale, $\tau_{\rm sf} \sim \tau_{\rm em}$. For much of the relevant parameter space, however, $\tau_{\rm sf}$ is likely to be much shorter than $\tau_{\rm em}$; see the discussion around Figure 1 in Lasky & Glampedakis (2016). For the two timescales to become comparable the magnetic ellipticity must be substantial, $\epsilon_B \gtrsim 10^{-3}$. For such a system the spin-flip timescale is minimized at a relatively high temperature, but the cooling in that regime is so rapid that the instability actually kicks in at a lower temperature where $\tau_{\rm sf}$ is significantly longer (and comparable to $\tau_{\rm em}$). In this scenario, millisecond magnetars harboring magnetic fields that are wound up to be sufficiently large are expected to have an $n < 3$ distribution. On the other hand, weaker fields in the core leading to smaller ellipticities may give rise to $n \approx 3$ magnetars.

Finally, it is worth pointing out that mechanisms that have been invoked to explain the anomalous braking indices of radio

pulsars are unlikely to be of relevance to the case at hand. The resurfacing of an initially "buried" magnetic field due to fallback material is a relatively slow process (dominated by the Ohmic-diffusion timescale $t \sim 1$–100 kyr; Viganò & Pons 2012) that is much longer than the timescales associated with short GRB remnants. Moreover, those calculations were done in the context of core-collapse supernovae where there is more fallback material to bury the field in the first place. Similarly, a gradual change in the stellar moment of inertia due to the onset of neutron superfluidity (Ho & Andersson 2012) could only take place in systems significantly older and colder than the ones considered here.

4. Conclusion

In this Letter, we make the first measurements of the braking index n of putative millisecond magnetars born in short gamma-ray bursts. Observations of X-ray plateaus following short gamma-ray bursts indicate the presence of ongoing energy injection, commonly attributed to the rotational evolution of a nascent neutron star. We show that the power-law exponent of the late-time ($\gtrsim 10^3$ s) decay of these curves can be directly related to the braking index; see Equation (2).

We show that the braking index of the magnetar in GRB 140903A is inconsistent with the fiducial value of $n = 3$ predicted for an unchanging, rotating dipolar magnetic field. However, as we propose in Section 3, there are a number of models that naturally explain this for millisecond magnetars. These include the presence of twisted components of the magnetic field in the magnetosphere (Section 3.1) or evolution of the angle between the magnetic axis and the star's rotation axis (Section 3.2). Another possibility is that the efficiency of converting spin-down energy into X-rays, η, evolves as a function of time; assuming $d\eta/dt < 0$, this would also lead to the inference of a sub-three braking index—see Section 2.1.

Perhaps what warrants more attention is the braking index for the millisecond magnetar born in GRB 130603B which, at $n = 2.9 \pm 0.1$, is consistent with the fiducial $n = 3$ value. This is the only empirically measured braking index consistent with $n = 3$. All sophisticated models of neutron star magnetosphere's tend to predict sub-three values for the braking index, especially when one considers those models relevant for the evolution of nascent stars born from binary neutron star mergers (see Section 3 for a detailed discussion). It is worth mentioning that ∼68% of the marginalized posterior for the braking index of the neutron star in GRB 130603B predicts $n < 3$.

It is tempting to read more into the X-ray light curve associated with GRB 130603B than we have done here. For example, the last *XMM* data point taken more than 6 days after the burst (see Figure 1) lies below almost all of the light curves generated from the posterior samples. It is therefore tempting to say that the braking index is actually evolving and that one should include a dn/dt term in the torque equation. However, there is simply not enough data at late times to warrant such a hypothesis. Clearly, to make such a claim one would want more data for times $t \gtrsim 10^6$ s, which will not be forthcoming for this GRB.

In lieu of more data for this particular GRB, we are left with potential statistical analyses of GRB light curves to determine braking indices of the population of millisecond magnetars born in short GRBs. We leave this to future work, although we note that a majority of short GRBs detected with *Swift* do not contain late-time observations from *XMM* or *Chandra* as with the GRBs analyzed here. Sensitivity limitations of *Swift*'s XRT limit the final data point to $t \lesssim 10^5$ s after the prompt emission, implying constraints on the braking index of magnetars born in such GRBs will come with commensurately larger uncertainties.

The analysis here can also be extended to light curve analyses of millisecond magnetars born in long GRBs and superluminous supernovae. Such analyses, however, are fraught with more difficulties than presented here. For example, both long GRBs and superluminous supernovae likely have denser and messier environments surrounding the initial explosion, implying extra complications in the spin-down torque from, for example, fallback accretion onto the newborn neutron star.

P.D.L. is grateful to Bing Zhang for useful conversations. We thank the referee for providing thorough feedback. P.D.L. is supported by ARC Future Fellowship FT160100112 and CoE CE170100004. P.D.L. and K.G. are supported by NewCompstar (a COST-funded Research Networking Programme).

References

Archibald, R. F., Gotthelf, E. V., Ferdman, R. D., et al. 2016, ApJL, 819, L16
Barthelmy, S. D., Barbier, L. M., Cummings, J. R., et al. 2005, SSRv, 120, 143
Barthelmy, S. D., Baumgartner, W. H., Cummings, J. R., et al. 2013, GCN, 14741, 1
Baumgarte, T. W., Shapiro, S. L., & Shibata, M. 2000, ApJL, 528, L29
Berger, E., Fong, W., & Chornock, R. 2013, ApJL, 774, L23
Braithwaite, J. 2009, MNRAS, 397, 763
Burrows, D. N., Hill, J. E., Nousek, J. A., et al. 2005, SSRv, 120, 165
Chatzopoulos, E., Wheeler, J. C., Vinko, J., Horvath, Z. L., & Nagy, A. 2013, ApJ, 773, 76
Clark, C. J., Pletsch, H. J., Wu, J., et al. 2016, ApJL, 832, L15
Contopoulos, I., & Spitkovsky, A. 2006, ApJ, 643, 1139
Cummings, J. R., Burrows, D. N., Evans, P. A., et al. 2014, GCN, 16763, 1
Cutler, C. 2002, PhRvD, 66, 084025
Cutler, C., & Jones, D. I. 2001, PhRvD, 63, 024002
de Pasquale, M., Maselli, A., & Cummings, J. R. 2014, GCN, 16767, 1
de Ugarte Postigo, A., Thöne, C. C., Rowlinson, A., et al. 2014, A&A, 563, A62
Fan, Y.-Z., Yu, Y.-W., Xu, D., et al. 2013, ApJL, 779, L25
Fong, W., Berger, E., Metzger, B. D., et al. 2014, ApJ, 780, 118
Goldreich, P. 1970, ApJL, 160, L11
Goldreich, P., & Julian, W. H. 1969, ApJ, 157, 869
Ho, W. C. G. 2016, MNRAS, 463, 489
Ho, W. C. G., & Andersson, N. 2012, NatPh, 8, 787
Inserra, C., Smartt, S. J., Gall, E. E. E., et al. 2016, ApJ, submitted (arXiv:1604.01226)
Kennea, J. A., Stroh, M. C., Burrows, D. N., et al. 2013, GCN, 14749, 1
Kiuchi, K., Kyutoku, K., Sekiguchi, Y., Shibata, M., & Wada, T. 2014, PhRvD, 90, 041502
Kiuchi, K., Yoshida, S., & Shibata, M. 2011, A&A, 532, A30
Lasky, P. D., & Glampedakis, K. 2016, MNRAS, 458, 1660
Lasky, P. D., Haskell, B., Ravi, V., Howell, E. J., & Coward, D. M. 2014, PhRvD, 89, 047302
Lü, H.-J., & Zhang, B. 2014, ApJ, 785, 74
Lü, H.-J., Zhang, B., Lei, W.-H., Li, Y., & Lasky, P. D. 2015, ApJ, 805, 89
Lyne, A. G., Jordan, C. A., Graham-Smith, F., et al. 2015, MNRAS, 446, 857
Marshall, F. E., Guillemot, L., Harding, A. K., et al. 2016, ApJL, 827, 39
Melandri, A., Baumgartner, W. H., Burrows, D. N., et al. 2013, GCN, 14735, 1
Melatos, A. 1997, MNRAS, 288, 1049
Metzger, B. D., Giannios, D., Thompson, T. A., Bucciantini, N., & Quataert, E. 2011, MNRAS, 413, 2031
Moriya, T. J., & Tauris, T. M. 2016, MNRAS, 460, L55
Nousek, J. A., Kouveliotou, C., Grupe, D., et al. 2006, ApJ, 642, 389
O'Brien, P. T., Willingale, R., Osborne, J., et al. 2006, ApJ, 647, 1213
Ostriker, J. P., & Gunn, J. E. 1969, ApJ, 157, 1395
Palmer, D. M., Barthelmy, S. D., Baumgartner, W. H., et al. 2014, GCN, 16768, 1

Rezzolla, L., Giacomazzo, B., Baiotti, L., et al. 2011, ApJL, 732, L6
Rowlinson, A., O'Brien, P. T., Metzger, B. D., Tanvir, N. R., & Levan, A. J. 2013, MNRAS, 430, 1061
Shapiro, S. L. 2000, ApJ, 544, 397
Spitkovsky, A. 2008, in AIP Conf. Ser. 983, 40 Years of Pulsars: Millisecond Pulsars, Magnetars and More, ed. C. Bassa et al. (Melville, NY: AIP), 20
Tanvir, N. R., Levan, A. J., Fruchter, A. S., et al. 2013, Natur, 500, 547
Thompson, C., Lyutikov, M., & Kulkarni, S. R. 2002, ApJ, 574, 332
Troja, E., Cusumano, G., O'Brien, P. T., et al. 2007, ApJ, 665, 599
Troja, E., Sakamoto, T., Cenko, S. B., et al. 2016, ApJ, 827, 102
Turolla, R., Zane, S., & Watts, A. L. 2015, RPPh, 78, 116901
Viganò, D., & Pons, J. A. 2012, MNRAS, 425, 2487
Zhang, B., Fan, Y. Z., Dyks, J., et al. 2006, ApJ, 642, 354
Zhang, B., & Mészáros, P. 2001, ApJL, 552, L35
Zhang, S., Jin, Z.-P., Wang, Y.-Z., & Wei, D.-M. 2017, ApJ, 835, 73